Engineering the Spatial Selectivity of Surfaces at the Nanoscale Using Particle Lithography Combined with Vapor Deposition of Organosilanes

Jie-Ren Li,[†] Kathie L. Lusker,[†] Jing-Jiang Yu,[‡] and Jayne C. Garno[†,*]

[†]Department of Chemistry and the Center for BioModular Multi-Scale Systems, Louisiana State University, 232 Choppin Hall, Baton Rouge, Louisiana 70803, and [‡]Nanotechnology Measurements Division, Agilent Technologies, Inc., 4330 West Chandler Boulevard, Chandler, Arizona 85226

ABSTRACT Particle lithography is a practical approach to generate millions of organosilane nanostructures on various surfaces, without the need for vacuum environments or expensive instrumentation. This report describes a stepwise chemistry route to prepare organosilane nanostructures and then apply the patterns as a spatially selective foundation to attach gold nanoparticles. Sites with thiol terminal groups were sufficiently small to localize the attachment of clusters of 2—5 nanoparticles. Basic steps such as centrifuging, drying, heating, and rinsing were used to generate arrays of regular nanopatterns. Close-packed films of monodisperse latex spheres can be used as an evaporative mask to spatially direct the placement of nanoscopic amounts of water on surfaces. Vapor phase organosilanes deposit selectively at areas of the surface containing water residues to generate nanostructures with regular thickness, geometry, and periodicity as revealed in atomic force microscopy images. The area of contact underneath the mesospheres is effectively masked for later synthetic steps, providing exquisite control of surface coverage and local chemistry. By judicious selection in designing the terminal groups of organosilanes, surface sites can be engineered at the nanoscale for building more complex structures. The density of the nanopatterns and surface coverage scale predictably with the diameter of the mesoparticle masks. The examples presented definitively illustrate the capabilities of using the chemistry of molecularly thin films of organosilanes to spatially define the selectivity of surfaces at very small size scales.

KEYWORDS: particle lithography · atomic force microscopy · nanopatterns · organosilanes · self-assembled monolayers · gold nanoparticles · nanolithography

Engineering the chemistry of surfaces at the nanoscale poses a significant challenge for nanotechnology.[1−5] Many strategies have emerged for nanoscale lithography, which hold promise for practical development of devices such as high density storage devices,[6,7] computer memory circuitry,[8,9] optoelectronic components,[10−12] and highly sensitive detectors.[12−14] In choosing nanolithography approaches for manufacturing devices, one of the most critical issues to be addressed is high throughput. Nanoscale technologies will undoubtedly require the ability to prepare millions of reproducible structures with high fidelity at low expense. The great promise of nanotechnology depends on the ability to organize materials at the nanoscale to generate designed assemblies that exhibit desirable properties. Molecular architectures with well-defined functionalities and composition will advance applications for molecular electronics[15−17] or biosensing.[18−20]

Particle lithography, which has also been referred to as nanosphere lithography or colloidal lithography, uses the close-packed arrangement of spherical particles to produce ordered arrays of regular nanostructures.[21,22] When dried, monodisperse spheres self-assemble into periodic structures with designed dimensions and interparticle spacing. Ordered arrays of mesospheres of colloidal silica or latex can then be used as structural templates or masks to guide the deposition of metals,[23,24] polymers,[25,26] catalysts,[27] nanoparticles,[28,29] self-assembled monolayers (SAMs),[30−33] and proteins.[34−37] We recently introduced a method to pattern organosilanes on surfaces such as glass, silicon wafers, mica, and gold using particle lithography combined with chemical vapor deposition.[33,38] Organosilanes bind to the interstitial areas of surfaces between masks of mesospheres at surface sites containing residues of water.

Well-defined self-assembled monolayers of organosilanes formed on oxide surfaces were first reported by Sagiv in 1980.[39] Since then, organosilanes have been widely applied to engineer surface properties and provide a versatile molecular platform for surface patterning and nanofabrication.[40−44]

*Address correspondence to jgarno@lsu.edu.

Received for review May 9, 2009 and accepted June 17, 2009.

Published online July 2, 2009.
10.1021/nn9004796 CCC: $40.75

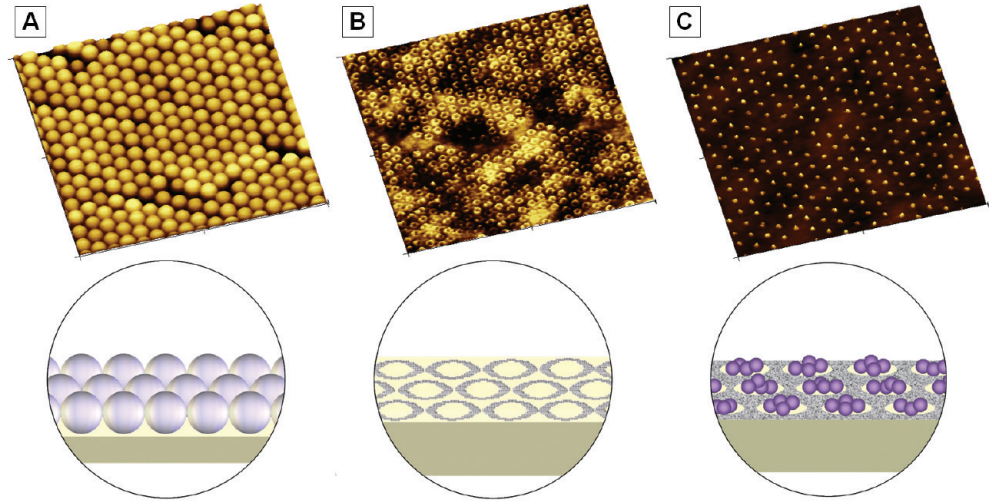

Figure 1. Snapshots of the key steps of particle lithography. (A) Evaporative mask of 200 nm latex, 4 × 4 μm² AFM contact-mode topograph. (B) Ring patterns of OTS formed on Si(111) viewed after latex removal (4 × 4 μm² topograph). (C) Arrays of gold nanoparticles attached to thiol-terminated patterns of organosilanes (4 × 4 μm²).

The interfacial functionalities of organosilane SAMs provide a way to tailor the chemistry of surfaces to attach various materials such as nanoparticles[45,46] and biomolecules.[18,47,48] The robust and covalent nature of organosilanes enables further steps of chemical modification to regulate surface chemistry.[49−52]

A range of lithography approaches have been developed to pattern organosilane monolayers such as photolithography,[53] UV-activated photochemistry,[54] electron beam lithography,[55,56] and microcontact printing.[57,58] Scanning probe lithography (SPL) approaches such as dip-pen nanolithography,[59,60] nanoshaving,[61,62] bias-induced lithography,[63] and constructive nanolithography[64−66] have also been applied to write nanopatterns of organosilane SAMs. Methods of SPL provide exquisite nanoscale resolution; however, the fabrication steps are time-consuming due to slow serial writing processes which are not easily scalable for the high throughput requirements of device manufacture.

Approaches based on successive steps of particle lithography, vapor deposition of organosilanes, and selective attachment of nanoparticles will be described in this report. The size, shape, and spacing of nanopatterns can be well-controlled at the nanoscale by the diameters of mesoparticle masks used for particle lithography. Surface selectivity can be engineered to define nanoscale sites for passivation or reactivity using well-defined functionalities of silanes. Engineered nanopatterns of adhesive and resistive silane SAMs provide exquisite surface selectivity at the nanoscale, which can be used as a foundation to direct the deposition of small clusters of nanoparticles. Surfaces can be designed to attach gold nanoparticles precisely to defined nanoscopic areas to form reproducible geometries and scalable surface coverage.

RESULTS AND DISCUSSION

Successive Steps for Defining Surface Chemistry *via* Particle Lithography. Solutions of monodisperse mesoparticles spontaneously self-assemble to form close-packed layers when dried on flat surfaces, as viewed in the AFM topography image of a film of 200 nm latex spheres (Figure 1A). The latex film is used as a mask for heated vapor deposition and exhibits hexagonal arrays of periodic, well-ordered domains with relatively few defects. The AFM topograph displays only the uppermost layer of the latex spheres, whereas the bottom layer in contact with the substrate actually serves as the mask for vapor deposition. Often the bottom layer will have fewer defects and better packing than the top surface because rows of particles are filled in from upper layers of spheres.[67,68] For the conditions tested, multiple layers of mesoparticles did not prevent vapors from intercalating between spheres to form surface patterns. After preparing masks of monodisperse mesoparticles, the surfaces were exposed to heated organosilane vapors in the next step. The time intervals for vapor exposure ranged from 6 to 24 h, depending on the nature of the organosilane molecules that were chosen. The mesospheres are removed in the next step by simple immersion in deionized water or solvents. Two properties of latex facilitate complete removal of the masks from the surface: the buoyancy of the spheres as well as the tendency for the spheres to swell and detach from the surface when liquid is added. Nanopatterns of organosilanes such as octadecyltrichlorosilane (OTS) remain securely attached to the surface, as shown by a representative AFM topograph in Figure 1B. An example of ring-shaped nanopatterns of OTS were produced on Si(111) *via* vapor deposition using a mask of 150 nm latex. The contours of the underlying silicon substrate somewhat predominate for the surface landscape for the molecularly thin structures; however, the

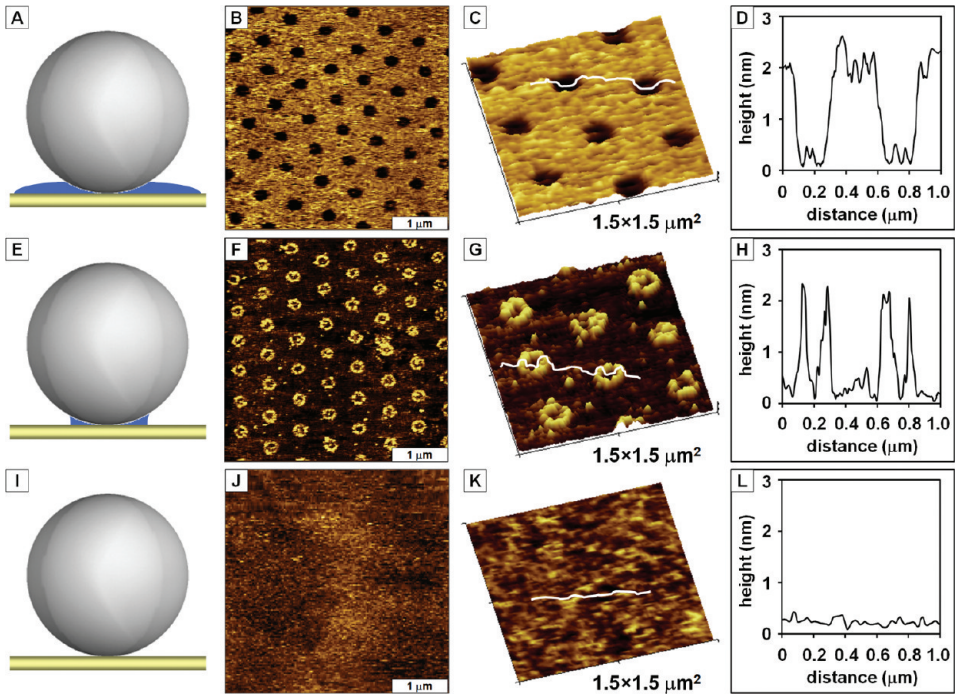

Figure 2. Sites of water residues determine the surface morphology of organosilane nanostructures. Nanopatterns were prepared using masks of 500 nm latex. (A) Interstitial areas between spheres are covered with water when the mask is dried briefly; (B) topography image of a porous OTS film on mica(0001) formed by briefly drying latex masks; (C) zoom-in view of B; (D) cursor profile for the line in C; (E) water meniscus forms at the base of spheres when masks are dried for several hours under ambient conditions; (F) topograph of an array of OTS ring patterns on mica(0001) generated with partially dried latex masks; (G) zoom-in view of F; (H) height profile for the cursor line in G; (I) latex masks which are dried completely have no water residues; (J) topograph indicates that no nanopatterns of OTS are generated on the surface when masks are dried completely; (K) zoom-in view of J; (L) cursor profile for the line in K.

periodic rows of ring nanopatterns can be clearly viewed spanning micrometer-sized areas of the surface. During vapor deposition, OTS molecules adsorb through steps of hydrolysis and condensation onto uncovered interstitial areas of the surface between latex spheres. The area of contact between the substrate and the base of the spheres is effectively masked to produce patterns with circular geometries. The latex masks are selectively and completely removed with the rinsing step, whereas the organosilanes remain covalently bound to the substrates.

After preparing organosilane nanostructures, additional steps can be accomplished to backfill uncovered areas of the surface with new molecules or nanomaterials. A second organosilane with a different terminal group can be used to backfill the bare areas of the substrates by a further successive chemical step, by immersing the binary patterned surface into solutions of other molecules or nanoparticles. An example is shown for gold nanoparticles deposited on nanopatterns of sulfur-terminated 3-mercaptopropyltrimethoxysilane (MPTMS) in Figure 1C. Because of the strong affinity between thiols and gold, gold nanoparticles adsorb selectively on the regions containing MPTMS. Arrays of gold nanoparticle clusters were generated on surfaces of Si(111) nanopatterned with OTS and MPTMS. The spacing and periodicity of the deposits of gold nanoparticles conform to the areas with MPTMS nanopatterns, and the areas of OTS provide an effective resist to prevent nonspecific binding in the surrounding areas. Full experimental details will be provided for each successive chemical step in further examples in this report.

Changes in Nanopattern Morphology with Different Drying Conditions of Masks. Molecules of OTS adsorb onto unmasked interstitial areas of the surface surrounding latex mesospheres where water residues are located.[33] The area of contact directly underneath the spheres is masked to produce patterns with circular geometries. The interpattern spacing is defined by the diameter of the latex; however, the nanopatterned areas of the surface, which were masked, are considerably smaller, with dimensions on the order of tens of nanometers. The amount of water present on the masked surfaces is affected by the drying intervals as well as the size of the mesospheres. Figure 2 demonstrates how the intervals for drying latex masks affect the morphology of organosilane nanopatterns on mica(0001). For substrates such as mica(0001), which contain relatively few hydroxyl groups, plasma treatment,[69] prehydrolysis of alkylsilanes,[70] and exposure of surfaces to water vapor[71] have been used to prepare films of organosilanes on mica. For latex masks that have been dried briefly (25 min), water is distributed homogeneously throughout areas of the surface to enable vapor phase assembly of OTS into the entire interstitial regions between latex particles (Figure 2A). The areas masked by the latex

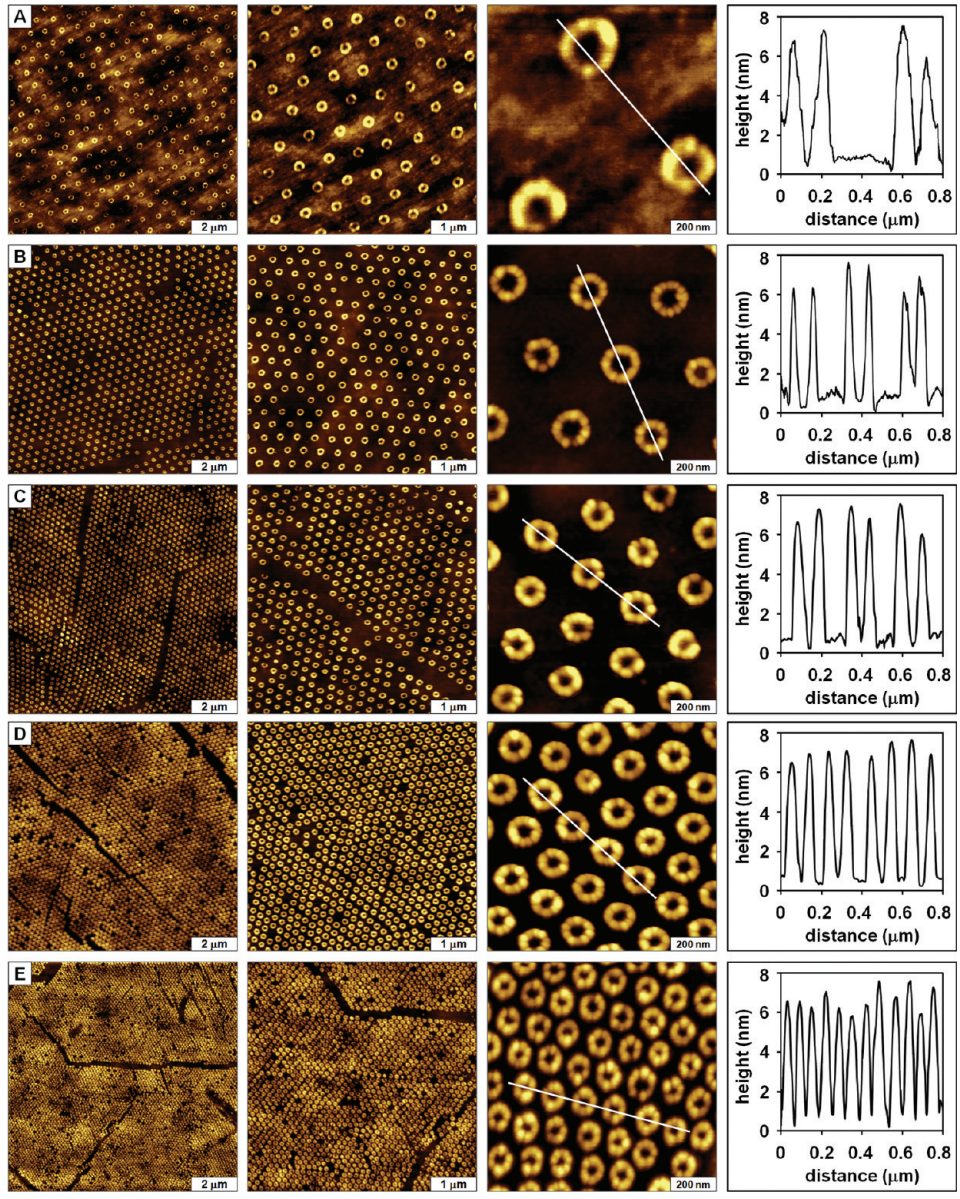

Figure 3. Changes in surface coverage and periodicity of organosilane nanopatterns using different mesosphere diameters. Tapping mode topography views of PEG-silane nanopatterns on Si(111) fabricated using (A) 500, (B) 300, (C) 200, (D) 150, and (E) 100 nm diameter latex.

spheres are protected from silane adsorption to produce a uniform OTS film of uncovered pore structures (Figure 2B,C). The thickness of the film measures 2.2 ± 0.4 nm, referencing the uncovered areas of the substrate as a baseline (Figure 2D). When mesoparticle masks are dried under ambient conditions for longer intervals (12 h), only tiny residues of water persist to form a circular meniscus in areas surrounding the base of latex spheres (Figure 2E). When the partially dried latex masks are exposed to OTS vapor, hydrolysis occurs only where water is present at the base of the spheres to form ring-shaped nanostructures of organosilanes as displayed in Figure 2F,G. The height of the rings measures 2.3 ± 0.3 nm, which closely matches the dimensions of the pore patterns within the OTS film (Figure 2H). For latex masks which were fully dried in an oven, no water is available to initiate hydrolysis of OTS (Figure 2I). After rinsing away the template latex particles for the oven-dried masks, no nanostructures are visible on the mica surface. There are no defined OTS nanostructures present in the AFM topograph of Figure 2J,K. The cursor profile in Figure 2L further shows that OTS structures did not form with templates that were dried in an oven.

Nanoscopic amounts of water are essential to initiate surface hydrolysis for organosilanes to bind to substrates. The distribution of water can be spatially controlled on surfaces using latex or colloidal silica mesoparticles as masks to direct the placement of water residues. The amount of water on surfaces is a critical parameter for controlling the sites for hydrolysis of organosilanes such as OTS, which can be regulated with

the drying intervals. When latex masks are dried briefly in ambient conditions, water is distributed homogeneously throughout areas of the surface to form an ultrathin film between mesoparticles. The organosilanes bind to the surface according to the arrangement and locations of water residues, essentially providing a fingerprint of the local distribution of water with AFM images of the nanopatterns. For mesoparticle masks that are dried under ambient conditions for longer intervals, water accumulates to form an exquisitely regular circular meniscus at the base of each latex sphere. As OTS vapor is introduced, silation only occurs where water is present to produce ring-shaped nanopatterns. Latex masks serve to define the locations of nanoscopic residues of water on gold surfaces which in turns spatially directs the sites for OTS to bind. The vapor deposition strategy for nanopatterning has been used successfully for patterning surfaces of mica(0001), Si(111), glass, and indium−tin oxide surfaces. Even the relatively hydrophobic surfaces of Au(111) can be successfully applied as substrates with particle lithography.[38]

Nanoscale Control of Periodicity and Surface Coverage. Changes of certain experimental parameters provide a means to systematically define the periodicity and surface coverage of nanostructures produced by particle lithography. For example, changing the diameter of the mesoparticle masks will alter the interpattern spacing as well as the size and surface densities of silane nanostructures. Predictably, a larger area of contact is observed for larger latex particles. An example is presented for arrays of 2-[methoxy(polyethyleneoxy)propyl]trimethoxysilane (PEG-silane) nanopatterns produced with latex masks of various diameters, shown by a series of AFM topographs in Figure 3. The surface density increases as the diameter of the latex spheres of the masks is changed from 500 nm to 300, 200, 150, and 100 nm for Figure 3A−E, respectively. For example, in the successive zoom-in views of Figure 3, the third column shows a 1 × 1 μm^2 view. The number of patterns progresses from 3 ring patterns per μm^2 in Figure 3A to 9, 19, 32, and 52 rings per μm^2 for Figure 3B−E, in succession. The periodicity of the ring patterns of PEG-silane can be measured with cursor line profiles and were found to closely match the expected diameters of the latex masks. The long-range order and organization of PEG-silane rings is apparent in the successive zoom-in views, with only a few defects produced by missing particles. The ring geometries of PEG-silane nanopatterns are remarkably consistent. Regardless of the latex diameters, the heights of the PEG ring patterns are quite uniform at the nanoscale, ranging from 6.4 to 7.1 nm in thickness. The unevenness of the height is likely produced by beading of water on the surface areas during the vapor deposition step, causing very slight irregularities in wetting of the surface at the nanoscale. The self-assembly process of various organosilanes has been reported to proceed *via* an island growth mechanism.[42,72−74] Adsorption of preorganized aggregates of organosilane molecules first occurs on surfaces where the nanoscopic residues of water are confined with latex masks. Slower adsorption processes continue to form a denser layer until silation is completed.

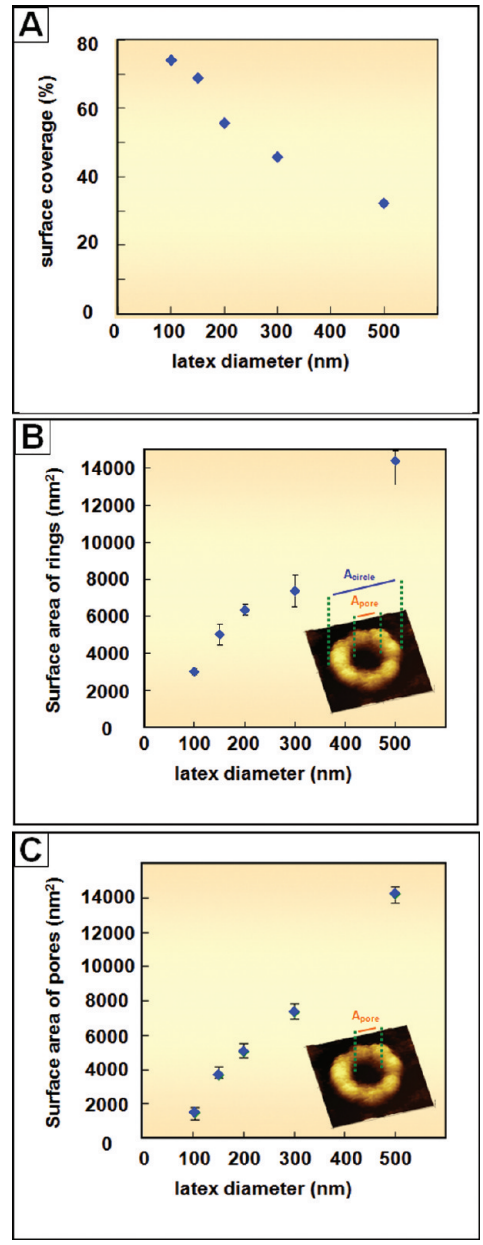

Figure 4. Analysis of the effect of latex diameter on (A) surface coverage of PEG silane nanostructures, (B) surface area of PEG silane ring patterns, and (C) surface area of uncovered pores.

Estimates of the surface coverage as well as the surface areas of the rings and pores of the PEG-silane nanopatterns are plotted in Figure 4. The charts demonstrate quantitatively that the surface area of the uncovered substrates as well as the areas covered by the ring patterns changes accordingly with mesoparticle diameters. The estimates were made using analysis of multiple representative images of different areas of

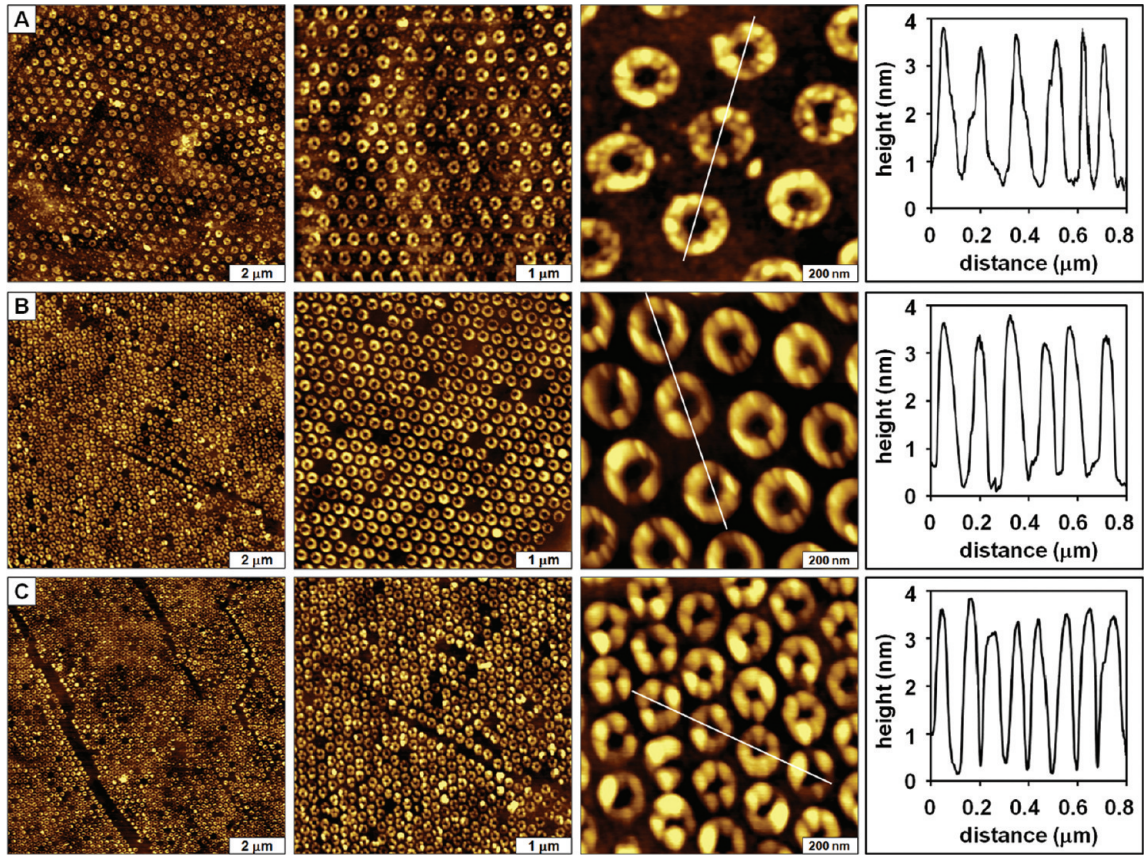

Figure 5. Periodic nanostructures of AAPTMS on Si(111) produced using particle lithography combined with heated vapor deposition. Tapping mode AFM topographs of AAPTMS nanopatterns produced with latex masks having periodicities of (A) 300 nm, (B) 200 nm, and (C) 150 nm.

the samples. The surface coverage for PEG-silane nanopatterns increases from 32 to 74% as the diameters of latex masks correspondingly change from 500 to 100 nm (Figure 4A). With smaller latex mesoparticles, close-packed masks offer sites to generate a larger number of nanopatterns, thus resulting in higher overall surface coverage of vapor-deposited silanes. The surface coverage within patterned areas of the PEG-silane rings scales accordingly with latex diameter as shown in Figure 4B, ranging from 3000 nm^2 (100 nm sphere diameter) to 14 000 nm^2 (500 nm diameter). The variation in the surface area of the rings results from changes in the size of the water meniscus formed at the base of spheres, defined by the areas wetted by nanoscopic amounts of water. Tiny residues of water are trapped near the latex particles to form a local meniscus surrounding the base of the spheres, and the size of this area increases progressively for larger diameter spheres. Larger particles enable more water to become trapped at the base of the spheres, forming a larger meniscus area to direct the surface attachment of organosilanes.

The uncovered surface areas of pores inside the PEG rings were observed to increase with larger latex diameters (Figure 4C). The pore sizes change from 1900 to 14 000 nm^2 as the latex diameter is increased from 100 to 500 nm. Measurements of the surface areas of uncovered pore sites within the PEG rings provide a way to assess the actual region of contact between latex spheres and the surface. The hydrodynamic radius of latex particles changes upon wetting, and the swelling of latex can cause the diameters of spheres to change at the nanoscale. As latex solutions are deposited and dried, the deformability of polystyrene latex results in changes for the area of contact between the latex spheres and the surface. For smaller latex spheres, overall more areas of the surface are masked.

Applicability of Particle Lithography for Different Terminal Moieties. Particle lithography was also applied successfully for patterning amine-terminated silanes. Nanopatterns of *N*-(6-aminohexyl)aminopropyltrimethoxysilane (AAPTMS) are shown in Figure 5 for various diameters of latex masks. Successive zoom-in views reveal that AAPTMS nanopatterns exhibit exquisitely uniform and regular ring morphologies, regardless of the different latex diameters (Figure 5A−C). The heights of the AAPTMS ring patterns are quite consistent, ranging from 3.2 to 3.7 nm. The periodicity corresponds closely to the dimensions of latex masks. The surface coverage and density of AAPTMS nanopatterns change accordingly with the diameters of mesoparticle masks used for particle lithography. The zoom-in images display a very slight unevenness of the height on the order of ±0.2 nm. This is likely caused by subtle differences in surface wetting during the vapor deposition step. The

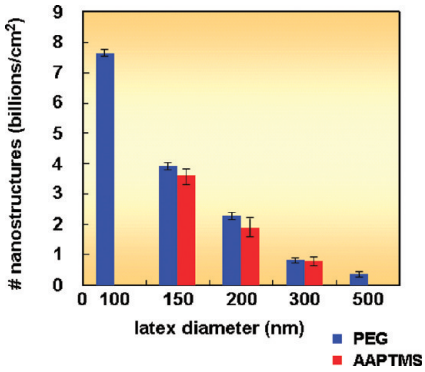

Figure 6. Comparison of the surface densities of PEG and AAPTMS nanostructures produced with different diameters of latex masks.

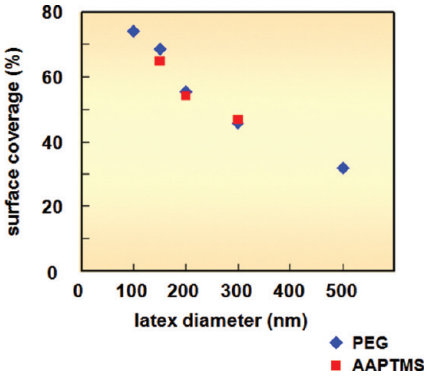

Figure 7. Differences between the percent surface coverage of PEG silane and AAPTMS nanopatterns fabricated using different mesoparticle diameters.

differences also may be attributable in part to AFM imaging artifacts. The widths of AFM probes can differ greatly at the nanoscale and contribute to broadening of lateral dimensions of very small surface features. However, it is more likely that the differences in overall surface area of the rings arise from natural differences in self-assembly and physical dimensions of AAPTMS *versus* PEG-silane.

The molecular structure, reactivity, and consequential surface assembly processes of organosilanes influence the resulting thickness of the nanostructures formed with organosilane SAMs. The longer polymer chains of PEG-silane molecules aggregate and interdigitate to form relatively larger clusters and proceed with a slower adsorption process on surfaces until silation is complete. The shorter backbone chains of the amine-terminated silane, AAPTMS, can self-catalyze the hydrolysis leading more aggressively to forming a multilayer compared to PEG-silane.[75−77] Due to interactions of head and tail groups between amine and silanol moieties, AAPTMS forms multilayers on surfaces, resulting in more disordered structures.[78,79] Zoom-in AFM views of AAPTMS nanopatterns reveal that the ring-shaped structures are composed of smaller clusters.

The changes in surface density were evaluated and compared as a function of latex diameter (Figure 6) for AAPTMS and PEG-silane nanostructures. Since the number of nanostructures is determined by the packing density of the latex spheres of the evaporative masks, the surface densities are quite consistent for AAPTMS and PEG-silane. The numbers of PEG rings range from 3.9×10^8 nanostructures per cm^2 for 500 nm spheres to as high as 7.6×10^9 for 100 nm latex. The steps of particle lithography combined with chemical vapor deposition are shown to reproducibly generate high surface densities with well-defined nanoscale geometries. Once the experimental conditions are optimized, dozens of samples prepared with the selected conditions exhibit similar nanoscale morphologies. Several samples were prepared to acquire data for the surface coverage and density, and the areas displayed in Figures 3 and 5 are representative of multiple areas and views throughout the sample surface.

Interestingly, AFM images display little difference at the nanoscale for the surface area of the rings of AAPTMS compared to PEG-silane nanopatterns (Figure 7). The surface coverage of nanopatterned surfaces with AAPTMS correspondingly changes with the size of the latex masks: 47, 54, and 65% for 300, 200, and 150 nm diameters, respectively. No obvious differences in surface coverage are apparent for AAPTMS *versus* PEG-silane ring nanopatterns, and there is considerable overlap in comparing the error bars of the chart. Considering that the molecular backbones and headgroups

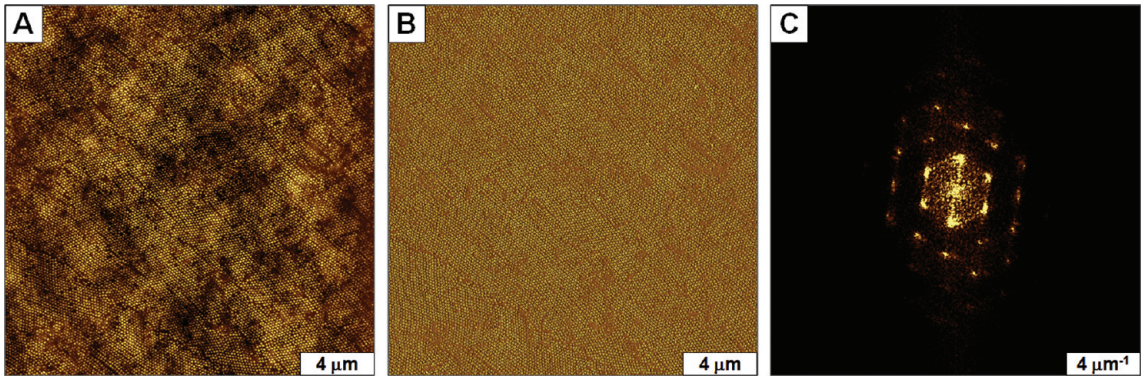

Figure 8. Wide area view of PEG-silane nanopatterns on silicon demonstrates the high throughput capabilities of particle lithography. (A) Topograph and (B) simultaneously acquired phase image acquired in ambient conditions with tapping mode AFM. (C) FFT analysis for the AFM topography image in A.

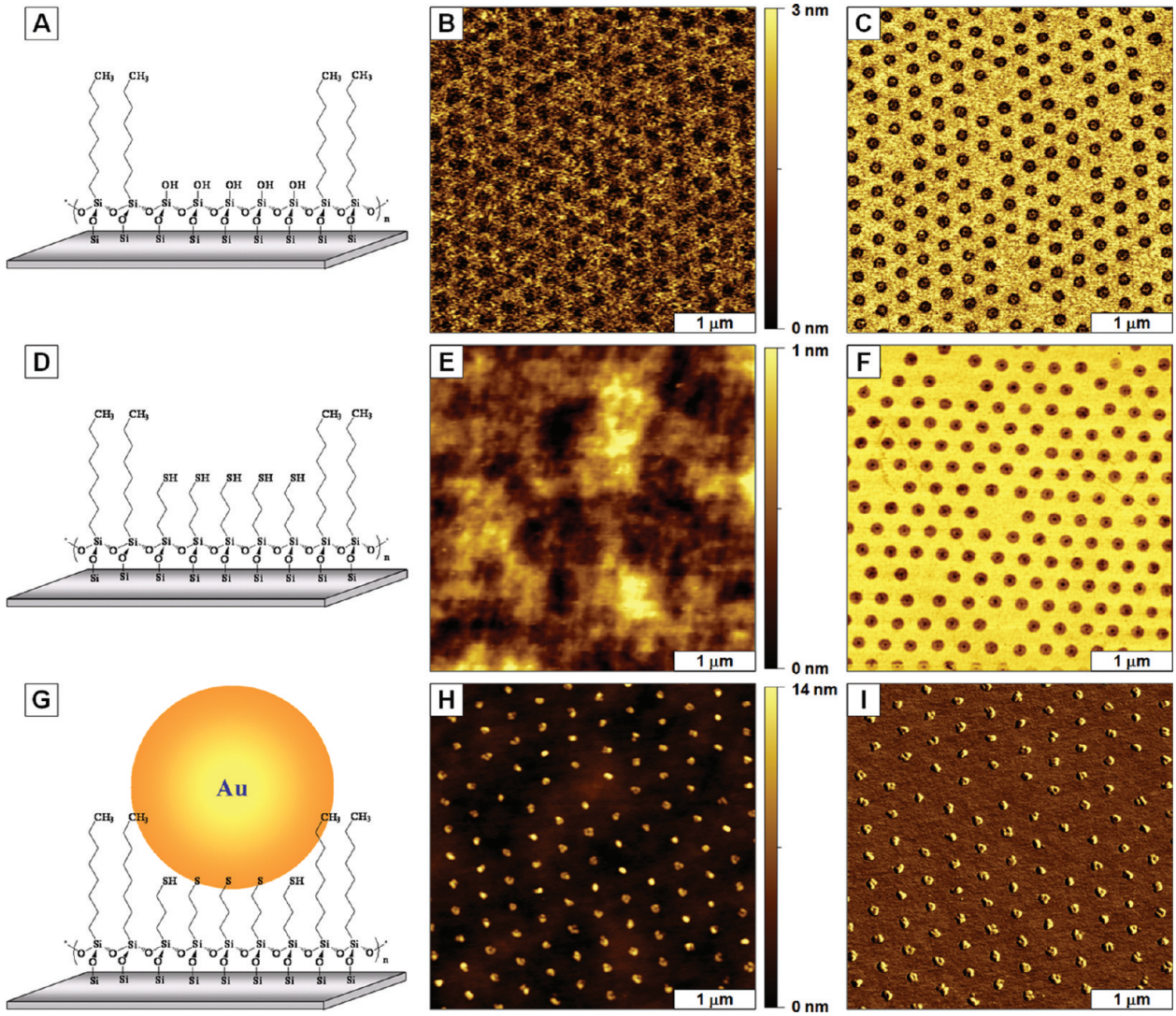

Figure 9. Sequence of chemical steps for selective attachment of gold nanoparticles on nanopatterns of organosilanes produced on a polished silicon wafer. (A) Nanopatterns of OTS produced by particle lithography; (B) topograph of an OTS film with pore structures produced with 300 nm latex; (C) corresponding lateral force image for B; (D) after depositing MPTMS onto uncovered pore areas within OTS; (E) topograph of a surface nanopatterned with OTS and MPTMS; (F) lateral force image for E; (G) gold nanoparticles attach selectively to areas with MPTMS; (H) topograph of arrays of gold nanoparticle clusters; (I) corresponding lateral force image for H.

of AAPTMS and PEG-silane are quite different, these results suggest that for defining the lateral dimensions of the surface patterns of the rings the critical factors are the locations and sites of water residues rather than the molecular architecture.

An example of the high throughput capabilities of particle lithography for fabricating organosilane nanopatterns is presented in Figure 8. The long-range order and organization of PEG-silane nanopatterns produced with 150 nm latex mesoparticles are apparent in the tapping mode AFM topograph, exhibiting relatively few defects over the 20 × 20 μm^2 scan area (Figure 8A). For a given fabrication condition, the surface morphologies were highly consistent and reproducible. The simultaneously acquired phase image in Figure 8B reveals more clearly that the PEG rings do not touch neighboring patterns. Phase images can sensitively distinguish differences in surface chemistry, elastic response, as well as edge effects.[80−83] Surfaces of PEG-silane rings exhibit a relatively uniform composition with a brighter contrast relative to the uncovered areas of silicon between the nanopatterns. A fast Fourier transform (FFT) analysis of the AFM topography frame with PEG rings is presented in Figure 8C. The FFT image clearly evidences the long-range order and hexagonal arrangement for arrays of PEG-silane rings.

The AFM images in Figure 8A,B also reveal the locations and placement of pattern defects. A few cracks are formed within the broader areas, which result from shrinkage of the latex masks during the drying step. The roughness of the underlying substrate morphology can also contribute to shifts in registry and vacancy areas. Surfaces which are atomically flat, such as mica(0001), generate a lower density of defects. Multiple approaches have been developed to produce

higher quality latex masks, and this subject has been previously reviewed.[84,85]

Spatial Selectivity for Generating Arrays of Gold Nanoparticles. Organosilane nanostructures can be used to define the placement of metal nanoparticles on surfaces. An example is presented in Figure 9 for the steps of patterning a resist silane of OTS, backfilling uncovered areas *via* an immersion step with a thiol-terminated organosilane, and the attachment of gold nanoparticles at defined sites using selected chemistries. In the first step, methyl-terminated patterns of OTS were generated either on silicon or on glass substrates using the previously described approach for vapor deposition through mesoparticle masks (Figure 9A). Arrays of OTS nanopatterns with pores of uncovered areas of substrate were produced as shown in Figure 9B (topograph) and 9C (lateral force image). Referencing the uncovered areas of the substrate as a baseline, the thickness of the OTS film is fairly even throughout the surface, exhibiting uniform coverage between pores. The dark areas of the lateral force image pinpoint the locations where latex particles were displaced. The differences in surface chemistry between the OTS film and the uncovered areas of the silicon substrate are apparent in Figure 9C. The brighter color of the OTS areas is quite uniform, indicating a homogeneous chemistry at the interface. Within this 4×4 μm^2 frame, there are 1500 nanopores providing 36% of the overall surface area for adsorption sites.

The uncovered areas of the silicon surface provide sites for a further chemical treatment to deposit a second organosilane with a solution immersion step. A short chain silane with thiol headgroups was deposited in the pore areas by 4 h immersion in a solution of 1 mM MPTMS in toluene (Figure 9D). The overall surface design therefore contains circular areas (*ca.* 68 nm diameter) presenting thiol groups surrounded by passivated areas with methyl-terminated OTS. The surface changes after the MPTMS immersion step are shown in Figure 9E,F. At this magnification, the shapes of the pores can no longer be clearly distinguished in the topography image. The height difference between OTS and MPTMS is too small in comparison to the roughness of the surface of polished silicon to be distinguished in the 4×4 μm^2 topography frame. The rms roughness measured 1.6 nm for the area shown. However, the differences in surface chemistry are clearly evident in the corresponding lateral force image of Figure 9F. The differences in adhesion between the tip and sample provide a sensitive map of the surface chemistry of the headgroups of OTS *versus* MPTMS. The brighter color of the lateral force image corresponds to the areas with methyl groups (OTS), whereas the thiol groups (MPTMS) inside the pores are darker. A tiny black dot at the center of the pores indicates that no MPTMS was deposited at the very center spot where the latex spheres made contact with the substrate.

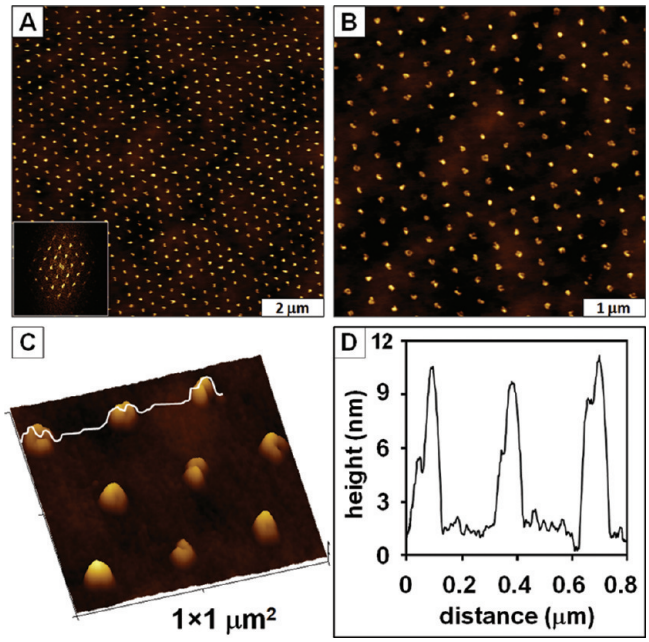

Figure 10. Successive magnified AFM views of the clusters of gold nanoparticles produced on Si(111). (A) Wide area topograph of periodic arrays of gold nanoparticles (10×10 μm^2); (B) close-up of the nanoparticle clusters (5×5 μm^2); (C) zoom-in view (1×1 μm^2); (D) cursor profile for the line in C.

This indicates that saturation coverage was not completely achieved for the pore areas during the immersion step.

The MPTMS nanopatterns can be used for selective deposition of gold nanoparticles *via* S−Au chemisorption (Figure 9G). Thiol-terminated MPTMS patterns provide sites to selectively confine and anchor gold nanoparticles to the surface. The methyl-terminated films of OTS provide a highly effective resist to prevent binding at boundary areas surrounding the circular areas of MPTMS. Due to the strong affinity between thiols and gold,[86−88] the gold nanoparticles adsorb selectively and uniformly at the regions with MPTMS, as demonstrated in the AFM images of Figure 9H,I. Within the 4×4 μm^2 topograph of Figure 9H, there are 1300 clusters composed of 2−5 gold nanoparticles. The corresponding lateral force image exhibits interesting changes for gold nanoparticles attached to MPTMS; the edges of individual nanoparticles can be resolved, providing a means to elucidate the shapes of individual nanoparticles (Figure 9I).

Successive zoom-in views of an array of gold nanoparticle clusters that were selectively adsorbed on a surface template of MPTMS nanopatterns surrounded by OTS are presented in Figure 10, for a sample prepared from masks of 300 nm latex mesospheres prepared on a glass slide. A representative 10×10 μm^2 topograph reveals the overall organization of the clusters of gold nanoparticles on the silicon substrate (Figure 10A). The overall morphologies and arrangement of the nanopatterns prepared on glass are quite similar at the nano-

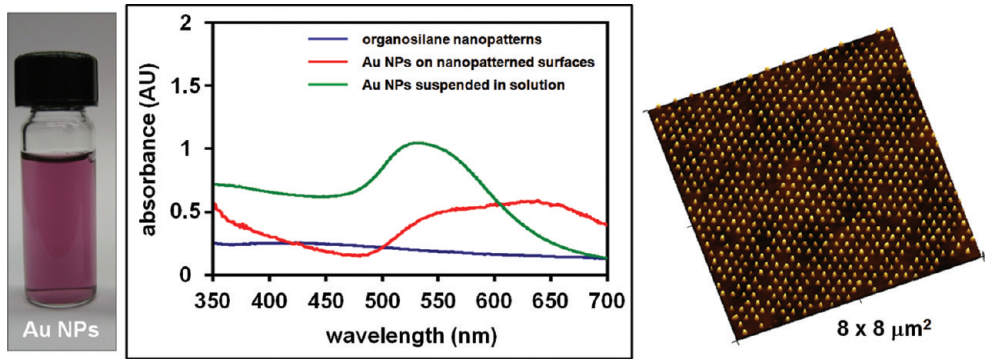

Figure 11. Optical properties of surface arrays of gold nanoparticle clusters investigated with UV−visible spectrophotometry. The red curve profiles the spectra of the gold nanoparticle solution (left). The blue curve corresponds to spectra of a nanopatterned surface of glass without gold nanoparticles. The green line displays spectra of the sample of gold nanoparticle clusters produced on glass (right).

scale to the views of nanopatterns prepared on polished silicon wafers shown in Figures 9H and 10A−C, illustrating the superb reproducibility of particle lithography steps, despite different substrates. The interstitial areas that are covered with methyl-terminated OTS provided a highly uniform and selective resist for preventing nanoparticle adsorption, whereas the pore regions filled with MPTMS define sites for attachment by presenting thiol groups to direct the binding of gold nanoparticles. A further close-up view in Figure 10B discloses the symmetric arrangement of 190 gold nanoparticle clusters, which cover 31% of the surface. Since the topography images clearly reveal the location and shapes of the gold nanoparticles, the number of nanoparticles within clusters can be obtained visually by examining multiple AFM images for different areas throughout the sample surface. The clusters are composed of 2−5 gold nanoparticles, approximately 13% of the clusters contain two nanoparticles. Within the 1 × 1 μm^2 area of Figure 10C, nine clusters of gold nanoparticles are viewed in the 3-D zoom-in frame. These images are representative of areas throughout the sample and demonstrate the exquisite spatial selectivity of organosilane nanopatterns. An average periodicity of 310 ± 14 nm was measured for the arrays of gold nanoparticles (Figure 10D), which corresponds closely to the dimensions of the latex masks (301 ± 4 nm). The average height of the gold nanostructures measured 13 ± 3 nm, with lateral dimensions ranging from 32 to 53 nm.

With spatially directed confinement of gold nanoparticles on glass surfaces, the arrays of nanoparticle clusters retain characteristic optical properties. Characterizations with ultraviolet−visible spectrophotometry were used to investigate the optical property of arrays of gold nanoparticle clusters (Figure 11). For comparative reference, UV−vis spectra were acquired for a gold nanoparticle solution and for a piece of glass with organosilane nanopatterns. A significant absorption peak was observed at 521 nm for the solution of suspended gold nanoparticles (green curve in Figure 11). The spectrum of the silane nanopatterns prepared on glass shown in Figure 11 (blue curve) does not exhibit any prominent absorption peaks in the visible region (350−700 nm) as a control sample. For the sample of gold nanoparticles adsorbed onto nanopatterns, a red shift up to a value of 632 nm was observed in the UV−vis spectra (red curve in Figure 11). The red spectral shift is attributable to changes in interparticle distance as gold nanoparticles assemble on the confined areas of the surface.[89−92]

CONCLUSION

Nanopatterns of organosilanes can be used effectively to define surface selectivity to designate the placement of other molecules and gold nanoparticles. Particle lithography provides advantages of high throughput for patterning organosilanes, furnishing nanoscale control of the surface coverage, geometry, and lateral dimensions of nanostructures. These results are a prelude to new directions for nanoscale patterning, using simple steps of bench chemistry that are accessible in most laboratories.

MATERIALS AND METHODS

Atomic Force Microscopy. Samples were characterized using either contact mode or acoustic AC mode AFM using either a model 5500 or 5600 LS scanning probe microscope (Agilent Technologies, Chandler, AZ). Rectangular silicon nitride cantilevers with force constants ranging from 21 to 98 N/m and an average resonance frequency of 165 kHz were used for AAC mode (tapping) characterizations (Nanosensors Lady's Island, SC). Contact mode AFM images were acquired using V-shaped cantilevers with oxide-sharpened silicon nitride probes, which had an average force constant of 0.5 N/m (Veeco Probes, Santa Barbara, CA). Images were processed using Gwyddion open source software, which is freely available on the Internet and supported by the Czech Metrology Institute.[93] Analysis of surface coverage was accomplished with multiple replicate images using Scanning Probe Image Processor (SPIP) software version 4.7.6 (Image Metrology, Denmark).

Preparation of Organosilane Nanopatterns. Particle lithography with vapor deposition was used to generate organosilane nanopatterns on surfaces, as previously reported.[33] Polished silicon wafers, Si(111) doped with boron (Virginia Semiconductor Inc., Fredericksburg, VA), and glass cover slides (Fisher Scientific, Pittsburgh, PA) were used as substrates. Substrates were cleaned by immersion in piranha solution for 1 h, which is a mixture of sulfuric acid and hydrogen peroxide at a (v/v) ratio of 3:1. Piranha solution is highly corrosive and should be handled carefully. Substrates were then rinsed copiously with deionized water and dried in air. Size-sorted polystyrene latex spheres (Thermo Scientific, Waltham, MA) were washed by centrifugation to remove contaminants such as charge stabilizer or surfactants. First, a small volume (200 μL) of size standard latex solution (1% w/v) was placed into a microcentrifuge tube. After centrifuging the latex suspension for 15 min at 14 000 rpm, a solid pellet was formed with a transparent supernatant. The supernatant was decanted and replaced with 100 μL of deionized water. The latex pellet was resuspended by vortex mixing, and a drop (20 μL) of the latex solution (2% w/v) was deposited on a clean substrate. The samples were dried in ambient conditions (25 C, relative humidity ~60%) to produce evaporative masks for particle lithography. As water evaporates during drying, capillary forces pull the mesospheres together to form organized crystalline layers on flat surfaces. During the drying step, most of the water evaporates and only tiny residues persist to form a meniscus surrounding the base of the spheres. Next, the substrates with latex masks were placed into a sealed reaction vessel containing 300 μL of the selected organosilane. A clean glass jar (100 mL) with a Teflon closure provided a suitable reaction vessel. Organosilanes such as OTS, AAPTMS, MPTMS, and PEG-silane were purchased from Gelest (Morrisville, PA) and used without further purification. To generate an organosilane vapor, the reaction vessel was placed in an oven and heated at 70−80 °C for at least 6 h under ambient pressure. During vapor deposition, organosilanes adsorbed to uncovered interstitial areas of the surface between latex spheres which contain water residues. The latex masks were removed completely by sonication and rinsing with ethanol and deionized water.

Deposition of a Second Organosilane by Solution Immersion. Areas of the surface that were not covered with nanopatterns could be backfilled with a second organosilane by solution immersion. Substrates with silane nanopatterns were immersed for 4 h in a toluene solution containing 1 mM of the chosen organosilane. Afterward, the samples were cleaned by sonication in toluene and ethanol for 15 min.

Attachment of Gold Nanoparticles to Organosilane Nanopatterns. Gold nanoparticles were synthesized according to a previously reported procedure.[94,95] The average size of the gold nanoparticles measured 12 ± 3 nm. Surfaces of silicon or glass containing binary nanopatterns of OTS and MPTMS were immersed in a solution of gold nanoparticles for 8 h. Afterward, the samples were briefly immersed in a sonicated solution of ethanol for 2 min and then rinsed further with ethanol and deionized water. Ultraviolet−visible spectra of gold nanoparticle arrays were recorded with a Varian Cary 50 UV−vis spectrophotometer (Palo Alto, CA).

Acknowledgment. The authors gratefully acknowledge support from the NSF-sponsored Center for BioModular Multi-Scale Systems at LSU, the ACS Petroleum Research Fund (PRF G43352-G5), the State of Louisiana Board of Regents, research competitiveness subprogram (LEQSF(2006-09)-RD-A-04), and the National Science Foundation Career program (CHE-0847291). J.-R.L. thanks Pfizer for a graduate fellowship in analytical chemistry.

REFERENCES AND NOTES

1. Xia, Y. N.; Whitesides, G. M. Soft Lithography. *Annu. Rev. Mater. Sci.* **1998**, *28*, 153–184.
2. Geissler, M.; Xia, Y. N. Patterning: Principles and Some New Developments. *Adv. Mater.* **2004**, *16*, 1249–1269.
3. Barth, J. V.; Costantini, G.; Kern, K. Engineering Atomic and Molecular Nanostructures at Surfaces. *Nature* **2005**, *437*, 671–679.
4. Rosi, N. L.; Mirkin, C. A. Nanostructures in Biodiagnostics. *Chem. Rev.* **2005**, *105*, 1547–1562.
5. Woodson, M.; Liu, J. Functional Nanostructures from Surface Chemistry Patterning. *Phys. Chem. Chem. Phys.* **2007**, *9*, 207–225.
6. Himpsel, F. J.; Ortega, J. E.; Mankey, G. J.; Willis, R. F. Magnetic Nanostructures. *Adv. Phys.* **1998**, *47*, 511–597.
7. Chou, S. Y. Patterned Magnetic Nanostructures and Quantized Magnetic Disks. *Proc. IEEE* **1997**, *85*, 652–671.
8. Tiwari, S.; Rana, F.; Hanafi, H.; Hartstein, A.; Crabbe, E. F.; Chan, K. A Silicon Nanocrystals Based Memory. *Appl. Phys. Lett.* **1996**, *68*, 1377–1379.
9. Joachim, C.; Gimzewski, J. K.; Aviram, A. Electronics Using Hybrid-Molecular and Mono-Molecular Devices. *Nature* **2000**, *408*, 541–548.
10. Duan, X. F.; Huang, Y.; Cui, Y.; Wang, J. F.; Lieber, C. M. Indium Phosphide Nanowires as Building Blocks for Nanoscale Electronic and Optoelectronic Devices. *Nature* **2001**, *409*, 66–69.
11. Wang, X. D.; Summers, C. J.; Wang, Z. L. Large-Scale Hexagonal-Patterned Growth of Aligned ZnO Nanorods for Nano-Optoelectronics and Nanosensor Arrays. *Nano Lett.* **2004**, *4*, 423–426.
12. Shipway, A. N.; Katz, E.; Willner, I. Nanoparticle Arrays on Surfaces for Electronic, Optical, and Sensor Applications. *ChemPhysChem* **2000**, *1*, 18–52.
13. Lin, Y. H.; Lu, F.; Tu, Y.; Ren, Z. F. Glucose Biosensors Based on Carbon Nanotube Nanoelectrode Ensembles. *Nano Lett.* **2004**, *4*, 191–195.
14. Kong, J.; Franklin, N. R.; Zhou, C. W.; Chapline, M. G.; Peng, S.; Cho, K. J.; Dai, H. J. Nanotube Molecular Wires as Chemical Sensors. *Science* **2000**, *287*, 622–625.
15. Zhou, C.; Deshpande, M. R.; Reed, M. A.; Jones, L.; Tour, J. M. Nanoscale Metal Self-Assembled Monolayer Metal Heterostructures. *Appl. Phys. Lett.* **1997**, *71*, 611–613.
16. Reed, M. A.; Zhou, C.; Muller, C. J.; Burgin, T. P.; Tour, J. M. Conductance of a Molecular Junction. *Science* **1997**, *278*, 252–254.
17. Wolkow, R. A. Controlled Molecular Adsorption on Silicon: Laying a Foundation for Molecular Devices. *Annu. Rev. Phys. Chem.* **1999**, *50*, 413–441.
18. Wadu-Mesthrige, K.; Xu, S.; Amro, N. A.; Liu, G. Y. Fabrication and Imaging of Nanometer-Sized Protein Patterns. *Langmuir* **1999**, *15*, 8580–8583.
19. Hyun, J.; Ahn, S. J.; Lee, W. K.; Chilkoti, A.; Zauscher, S. Molecular Recognition-Mediated Fabrication of Protein Nanostructures by Dip-Pen Lithography. *Nano Lett.* **2002**, *2*, 1203–1207.
20. Hrapovic, S.; Liu, Y. L.; Male, K. B.; Luong, J. H. T. Electrochemical Biosensing Platforms Using Platinum Nanoparticles and Carbon Nanotubes. *Anal. Chem.* **2004**, *76*, 1083–1088.
21. Haynes, C. L.; Van Duyne, R. P. Nanosphere Lithography: A Versatile Nanofabrication Tool for Studies of Size-Dependent Nanoparticle Optics. *J. Phys. Chem. B* **2001**, *105*, 5599–5611.
22. Xia, Y. N.; Gates, B.; Yin, Y. D.; Lu, Y. Monodispersed Colloidal Spheres: Old Materials with New Applications. *Adv. Mater.* **2000**, *12*, 693–713.
23. Tessier, P.; Velev, O. D.; Kalambur, A. T.; Lenhoff, A. M.; Rabolt, J. F.; Kaler, E. W. Structured Metallic Films for Optical and Spectroscopic Applications *via* Colloidal Crystal Templating. *Adv. Mater.* **2001**, *13*, 396–400.
24. Jiang, P.; McFarland, M. J. Large-Scale Fabrication of Wafer-Size Colloidal Crystals, Macroporous Polymers and Nanocomposites by Spin-Coating. *J. Am. Chem. Soc.* **2004**, *126*, 13778–13786.
25. Jiang, P.; Hwang, K. S.; Mittleman, D. M.; Bertone, J. F.; Colvin, V. L. Template-Directed Preparation of Macroporous Polymers with Oriented and Crystalline Arrays of Voids. *J. Am. Chem. Soc.* **1999**, *121*, 11630–11637.
26. Briseno, A. L.; Han, S. B.; Rauda, I. E.; Zhou, F. M.; Toh, C. S.; Nemanick, E. J.; Lewis, N. S. Electrochemical Polymerization of Aniline Monomers Infiltrated into Well-Ordered

Truncated Eggshell Structures of Polyelectrolyte Multilayers. *Langmuir* **2004**, *20*, 219–226.
27. Gustavsson, M.; Fredriksson, H.; Kasemo, B.; Jusys, Z.; Kaiser, J.; Jun, C.; Behm, R. J. Nanostructured Platinum-on-Carbon Model Electrocatalysts Prepared by Colloidal Lithography. *J. Electroanal. Chem.* **2004**, *568*, 371–377.
28. Lewandowski, B. R.; Kelley, A. T.; Singleton, R.; Li, J.-R.; Lowry, M.; Warner, I. M.; Garno, J. C. Nanostructures of Cysteine-Coated CdS Nanoparticles Produced with "Two-Particle" Lithography. *J. Phys. Chem. C* **2009**, *113*, 5933–5940.
29. Chen, J. X.; Liao, W. S.; Chen, X.; Yang, T. L.; Wark, S. E.; Son, D. H.; Batteas, J. D.; Cremer, P. S. Evaporation-Induced Assembly of Quantum Dots into Nanorings. *ACS Nano* **2009**, *3*, 173–180.
30. McLellan, J. M.; Geissler, M.; Xia, Y. N. Edge Spreading Lithography and its Application to the Fabrication of Mesoscopic Gold and Silver Rings. *J. Am. Chem. Soc.* **2004**, *126*, 10830–10831.
31. Geissler, M.; McLellan, J. M.; Chen, J. Y.; Xia, Y. N. Side-by-Side Patterning of Multiple Alkanethiolate Monolayers on Gold by Edge-Spreading Lithography. *Angew. Chem., Int. Ed.* **2005**, *44*, 3596–3600.
32. Bae, C.; Shin, H. J.; Moon, J.; Sung, M. M. Contact Area Lithography (CAL): A New Approach to Direct Formation of Nanometric Chemical Patterns. *Chem. Mater.* **2006**, *18*, 1085–1088.
33. Li, J. R.; Garno, J. C. Elucidating the Role of Surface Hydrolysis in Preparing Organosilane Nanostructures *via* Particle Lithography. *Nano Lett.* **2008**, *8*, 1916–1922.
34. Garno, J. C.; Amro, N. A.; Wadu-Mesthrige, K.; Liu, G. Y. Production of Periodic Arrays of Protein Nanostructures Using Particle Lithography. *Langmuir* **2002**, *18*, 8186–8192.
35. Cai, Y. G.; Ocko, B. M. Large-Scale Fabrication of Protein Nanoarrays Based on Nanosphere Lithography. *Langmuir* **2005**, *21*, 9274–9279.
36. Li, J. R.; Henry, G. C.; Garno, J. C. Fabrication of Nanopatterned Films of Bovine Serum Albumin and Staphylococcal Protein A Using Latex Particle Lithography. *Analyst* **2006**, *131*, 244–250.
37. Ngunjiri, J. N.; Daniels, S. L.; Li, J. R.; Serem, W. K.; Garno, J. C. Controlling the Surface Coverage and Arrangement of Proteins Using Particle Lithography. *Nanomedicine* **2008**, *3*, 529–541.
38. Li, J. R.; Garno, J. C. Nanostructures of Octadecyltrisiloxane Self-Assembled Monolayers Produced on Au(111) Using Particle Lithography. *ACS Appl. Mater. Interfaces* **2009**, *1*, 969–976.
39. Sagiv, J. Organized Monolayers by Adsorption 0.1. Formation and Structure of Oleophobic Mixed Monolayers on Solid-Surfaces. *J. Am. Chem. Soc.* **1980**, *102*, 92–98.
40. Ulman, A. Formation and Structure of Self-Assembled Monolayers. *Chem. Rev.* **1996**, *96*, 1533–1554.
41. Love, J. C.; Estroff, L. A.; Kriebel, J. K.; Nuzzo, R. G.; Whitesides, G. M. Self-Assembled Monolayers of Thiolates on Metals as a Form of Nanotechnology. *Chem. Rev.* **2005**, *105*, 1103–1169.
42. Onclin, S.; Ravoo, B. J.; Reinhoudt, D. N. Engineering Silicon Oxide Surfaces Using Self-Assembled Monolayers. *Angew. Chem., Int. Ed.* **2005**, *44*, 6282–6304.
43. Brzoska, J. B.; Benazouz, I.; Rondelez, F. Silanization of Solid Substrates—A Step toward Reproducibility. *Langmuir* **1994**, *10*, 4367–4373.
44. Hozumi, A.; Ushiyama, K.; Sugimura, H.; Takai, O. Fluoroalkylsilane Monolayers Formed by Chemical Vapor Surface Modification on Hydroxylated Oxide Surfaces. *Langmuir* **1999**, *15*, 7600–7604.
45. Grabar, K. C.; Allison, K. J.; Baker, B. E.; Bright, R. M.; Brown, K. R.; Freeman, R. G.; Fox, A. P.; Keating, C. D.; Musick, M. D.; Natan, M. J. Two-Dimensional Arrays of Colloidal Gold Particles: A Flexible Approach to Macroscopic Metal Surfaces. *Langmuir* **1996**, *12*, 2353–2361.
46. Gao, Y. F.; Koumoto, K. Bioinspired Ceramic Thin Film Processing: Present Status and Future Perspectives. *Cryst. Growth Des.* **2005**, *5*, 1983–2017.
47. Chrisey, L. A.; Lee, G. U.; Oferrall, C. E. Covalent Attachment of Synthetic DNA to Self-Assembled Monolayer Films. *Nucleic Acids Res.* **1996**, *24*, 3031–3039.
48. Mooney, J. F.; Hunt, A. J.; McIntosh, J. R.; Liberko, C. A.; Walba, D. M.; Rogers, C. T. Patterning of Functional Antibodies and Other Proteins by Photolithography of Silane Monolayers s. *Proc. Natl. Acad. Sci. U.S.A.* **1996**, *93*, 12287–12291.
49. Wasserman, S. R.; Tao, Y. T.; Whitesides, G. M. Structure and Reactivity of Alkylsiloxane Monolayers Formed by Reaction of Alkyltrichlorosilanes on Silicon Substrates. *Langmuir* **1989**, *5*, 1074–1087.
50. Balachander, N.; Sukenik, C. N. Monolayer Transformation by Nucleophilic-Substitution—Applications to the Creation of New Monolayer Assemblies. *Langmuir* **1990**, *6*, 1621–1627.
51. Maoz, R.; Cohen, S. R.; Sagiv, J. Nanoelectrochemical Patterning of Monolayer Surfaces: toward Spatially Defined Self-Assembly of Nanostructures. *Adv. Mater.* **1999**, *11*, 55–61.
52. Killampalli, A. S.; Ma, P. F.; Engstrom, J. R. The Reaction of Tetrakis(dimethylamido)titanium with Self-Assembled Alkyltrichlorosilane Monolayers Possessing $-OH$, $-NH_2$, and $-CH_3$ Terminal Groups. *J. Am. Chem. Soc.* **2005**, *127*, 6300–6310.
53. Dulcey, C. S.; Georger, J. H.; Krauthamer, V.; Stenger, D. A.; Fare, T. L.; Calvert, J. M. Deep UV Photochemistry of Chemisorbed Monolayers—Patterned Coplanar Molecular Assemblies. *Science* **1991**, *252*, 551–554.
54. Brandow, S. L.; Chen, M. S.; Aggarwal, R.; Dulcey, C. S.; Calvert, J. M.; Dressick, W. J. Fabrication of Patterned Amine Reactivity Templates Using 4-Chloromethylphenylsiloxane Self-Assembled Monolayer Films. *Langmuir* **1999**, *15*, 5429–5432.
55. Lercel, M. J.; Redinbo, G. F.; Pardo, F. D.; Rooks, M.; Tiberio, R. C.; Simpson, P.; Craighead, H. G.; Sheen, C. W.; Parikh, A. N.; Allara, D. L. Electron-Beam Lithography with Monolayers of Alkylthiols and Alkylsiloxanes. *J. Vac. Sci. Technol., B* **1994**, *12*, 3663–3667.
56. Lercel, M. J.; Craighead, H. G.; Parikh, A. N.; Seshadri, K.; Allara, D. L. Sub-10 nm Lithography with Self-Assembled Monolayers. *Appl. Phys. Lett.* **1996**, *68*, 1504–1506.
57. Xia, Y. N.; Mrksich, M.; Kim, E.; Whitesides, G. M. Microcontact Printing of Octadecylsiloxane on the Surface of Silicon Dioxide and Its Application in Microfabrication. *J. Am. Chem. Soc.* **1995**, *117*, 9576–9577.
58. Wang, D. W.; Thomas, S. G.; Wang, K. L.; Xia, Y. N.; Whitesides, G. M. Nanometer Scale Patterning and Pattern Transfer on Amorphous Si, Crystalline Si, and SiO_2 Surfaces Using Self-Assembled Monolayers. *Appl. Phys. Lett.* **1997**, *70*, 1593–1595.
59. Ivanisevic, A.; Mirkin, C. A. "Dip-Pen" Nanolithography on Semiconductor Surfaces. *J. Am. Chem. Soc.* **2001**, *123*, 7887–7889.
60. Jung, H.; Kulkarni, R.; Collier, C. P. Dip-Pen Nanolithography of Reactive Alkoxysilanes on Glass. *J. Am. Chem. Soc.* **2003**, *125*, 12096–12097.
61. Jourdan, J. S.; Cruchon-Dupeyrat, S. J.; Huan, Y.; Kuo, P. K.; Liu, G. Y. Imaging Nanoscopic Elasticity of Thin Film Materials by Atomic Force Microscopy: Effects of Force Modulation Frequency and Amplitude. *Langmuir* **1999**, *15*, 6495–6504.
62. Headrick, J. E.; Armstrong, M.; Cratty, J.; Hammond, S.; Sheriff, B. A.; Berrie, C. L. Nanoscale Patterning of Alkyl Monolayers on Silicon Using the Atomic Force Microscope. *Langmuir* **2005**, *21*, 4117–4122.
63. Gu, J. H.; Yam, C. M.; Li, S.; Cai, C. Z. Nanometric Protein Arrays on Protein-Resistant Monolayers on Silicon Surfaces. *J. Am. Chem. Soc.* **2004**, *126*, 8098–8099.
64. Maoz, R.; Frydman, E.; Cohen, S. R.; Sagiv, J. Constructive Nanolithography: Site-Defined Silver Self-Assembly on

Nanoelectrochemically Patterned Monolayer Templates. *Adv. Mater.* **2000**, *12*, 424–429.
65. Maoz, R.; Frydman, E.; Cohen, S. R.; Sagiv, J. "Constructive Nanolithography": Inert Monolayers as Patternable Templates for *In-Situ* Nanofabrication of Metal-Semiconductor-Organic Surface Structures—Generic Approach. *Adv. Mater.* **2000**, *12*, 725–731.
66. Hoeppener, S.; Maoz, R.; Sagiv, J. Constructive Microlithography: Electrochemical Printing of Monolayer Template Patterns Extends Constructive Nanolithography to the Micrometer−Millimeter Dimension Range. *Nano Lett.* **2003**, *3*, 761–767.
67. Denkov, N. D.; Velev, O. D.; Kralchevsky, P. A.; Ivanov, I. B.; Yoshimura, H.; Nagayama, K. Mechanism of Formation of 2-Dimensional Crystals from Latex-Particles on Substrates. *Langmuir* **1992**, *8*, 3183–3190.
68. Prevo, B. G.; Velev, O. D. Controlled, Rapid Deposition of Structured Coatings from Micro- and Nanoparticle Suspensions. *Langmuir* **2004**, *20*, 2099–2107.
69. Kim, S.; Christenson, H. K.; Curry, J. E. The Effect of Humidity on the Stability of an Octadecyltriethoxysilane Monolayer Self-Assembled on Untreated and Plasma-Treated Mica. *Langmuir* **2002**, *18*, 2125–2129.
70. Kessel, C. R.; Granick, S. Formation and Characterization of a Highly Ordered and Well-Anchored Alkylsilane Monolayer on Mica by Self-Assembly. *Langmuir* **1991**, *7*, 532–538.
71. Schwartz, D. K.; Steinberg, S.; Israelachvili, J.; Zasadzinski, J. A. N. Growth of a Self-Assembled Monolayer by Fractal Aggregation. *Phys. Rev. Lett.* **1992**, *69*, 3354–3357.
72. Bierbaum, K.; Grunze, M.; Baski, A. A.; Chi, L. F.; Schrepp, W.; Fuchs, H. Growth of Self-Assembled *N*-Alkyltrichlorosilane Films on Si(100) Investigated by Atomic-Force Microscopy. *Langmuir* **1995**, *11*, 2143–2150.
73. Banga, R.; Yarwood, J.; Morgan, A. M.; Evans, B.; Kells, J. FTIR and AFM Studies of the Kinetics and Self-Assembly of Alkyltrichlorosilanes and (Perfluoroalkyl)trichlorosilanes onto Glass and Silicon. *Langmuir* **1995**, *11*, 4393–4399.
74. Vallant, T.; Brunner, H.; Mayer, U.; Hoffmann, H.; Leitner, T.; Resch, R.; Friedbacher, G. Formation of Self-Assembled Octadecylsiloxane Monolayers on Mica and Silicon Surfaces Studied by Atomic Force Microscopy and Infrared Spectroscopy. *J. Phys. Chem. B* **1998**, *102*, 7190–7197.
75. Vandenberg, E. T.; Bertilsson, L.; Liedberg, B.; Uvdal, K.; Erlandsson, R.; Elwing, H.; Lundstrom, I. Structure of 3-Aminopropyl Triethoxy Silane on Silicon-Oxide. *J. Colloid Interface Sci.* **1991**, *147*, 103–118.
76. Horr, T. J.; Arora, P. S. Determination of the Acid-Base Properties for 3-Amino, 3-Chloro and 3-Mercaptopropyltrimethoxysilane Coatings on Silica Surfaces by XPS. *Colloids Surf., A* **1997**, *126*, 113–121.
77. Kristensen, E. M. E.; Nederberg, F.; Rensmo, H.; Bowden, T.; Hilborn, J.; Siegbahn, H. Photoelectron Spectroscopy Studies of the Functionalization of a Silicon Surface with a Phosphorylcholine-Terminated Polymer Grafted onto (3-Aminopropyl)trimethoxysilane. *Langmuir* **2006**, *22*, 9651–9657.
78. Fadeev, A. Y.; McCarthy, T. J. Self-Assembly is not the Only Reaction Possible between Alkyltrichlorosilanes and Surfaces: Monomolecular and Oligomeric Covalently Attached Layers of Dichloro- and Trichloroalkylsilanes on Silicon. *Langmuir* **2000**, *16*, 7268–7274.
79. Howarter, J. A.; Youngblood, J. P. Optimization of Silica Silanization by 3-Aminopropyltriethoxysilane. *Langmuir* **2006**, *22*, 11142–11147.
80. Radmacher, M.; Tilmann, R. W.; Gaub, H. E. Imaging Viscoelasticity by Force Modulation with the Atomic Force Microscope. *Biophys. J.* **1993**, *64*, 735–742.
81. Magonov, S. N.; Reneker, D. H. Characterization of Polymer Surfaces with Atomic Force Microscopy. *Annu. Rev. Mater. Sci.* **1997**, *27*, 175–222.
82. Finot, M. O.; McDermott, M. T. High-Resolution Chemical Mapping of Surface Bound Functional Groups with Tapping-Mode Scanning Force Microscopy. *J. Am. Chem. Soc.* **1997**, *119*, 8564–8565.
83. Garcia, R.; Perez, R. Dynamic Atomic Force Microscopy Methods. *Surf. Sci. Rep.* **2002**, *47*, 197–301.
84. Yang, S.-M.; Jang, S. G.; Choi, D.-G.; Kim, S.; Yu, H. Y. Nanomachining by Colloidal Lithography. *Small* **2006**, *2*, 458–475.
85. Hoa, M. L. K.; Lu, M.; Zhang, Y. Preparation of Porous Materials with Ordered Hole Structure. *Adv. Colloid Interface Sci.* **2006**, *121*, 9–23.
86. Freeman, R. G.; Grabar, K. C.; Allison, K. J.; Bright, R. M.; Davis, J. A.; Guthrie, A. P.; Hommer, M. B.; Jackson, M. A.; Smith, P. C.; Walter, D. G.; Natan, M. J. Self-Assembled Metal Colloid Monolayers—An Approach to SERS Substrates. *Science* **1995**, *267*, 1629–1632.
87. Westcott, S. L.; Oldenburg, S. J.; Lee, T. R.; Halas, N. J. Formation and Adsorption of Clusters of Gold Nanoparticles onto Functionalized Silica Nanoparticle Surfaces. *Langmuir* **1998**, *14*, 5396–5401.
88. He, H. X.; Zhang, H.; Li, Q. G.; Zhu, T.; Li, S. F. Y.; Liu, Z. F. Fabrication of Designed Architectures of Au Nanoparticles on Solid Substrate with Printed Self-Assembled Monolayers as Templates. *Langmuir* **2000**, *16*, 3846–3851.
89. Rechberger, W.; Hohenau, A.; Leitner, A.; Krenn, J. R.; Lamprecht, B.; Aussenegg, F. R. Optical Properties of Two Interacting Gold Nanoparticles. *Opt. Commun.* **2003**, *220*, 137–141.
90. Daniel, M. C.; Astruc, D. Gold Nanoparticles: Assembly, Supramolecular Chemistry, Quantum-Size-Related Properties, and Applications toward Biology, Catalysis, and Nanotechnology. *Chem. Rev.* **2004**, *104*, 293–346.
91. Murphy, C. J.; San, T. K.; Gole, A. M.; Orendorff, C. J.; Gao, J. X.; Gou, L.; Hunyadi, S. E.; Li, T. Anisotropic Metal Nanoparticles: Synthesis, Assembly, and Optical Applications. *J. Phys. Chem. B* **2005**, *109*, 13857–13870.
92. Lin, S.; Li, M.; Dujardin, E.; Girard, C.; Mann, S. One-Dimensional Plasmon Coupling by Facile Self-Assembly of Gold Nanoparticles into Branched Chain Networks. *Adv. Mater.* **2005**, *17*, 2553–2559.
93. Klapetek, P. N. D. *Gwyddion*; Czech Metrology Institute, Czech Republic, 2007, http://gwyddion.net/.
94. Grabar, K. C.; Freeman, R. G.; Hommer, M. B.; Natan, M. J. Preparation and Characterization of Au Colloid Monolayers. *Anal. Chem.* **1995**, *67*, 735–743.
95. Grabar, K. C.; Brown, K. R.; Keating, C. D.; Stranick, S. J.; Tang, S. L.; Natan, M. J. Nanoscale Characterization of Gold Colloid Monolayers: A Comparison of four Techniques. *Anal. Chem.* **1997**, *69*, 471–477.